



Mass spectrometric fragmentation patterns discriminate C1- and C4-oxidised cello-oligosaccharides from their non-oxidised and reduced forms

Peicheng Sun, Matthias Frommhagen, Maloe Kleine Haar, Gijs van Erven, Edwin J. Bakx, Willem J.H. van Berkel, Mirjam A. Kabel*

Laboratory of Food Chemistry, Wageningen University and Research, Bornse Weilanden 9, 6708 WG Wageningen, the Netherlands



ARTICLE INFO

Keywords:

Lignocellulose
Biomass conversion
LPMOs
Cello-oligosaccharides
HILIC-ESI-CID-MS/MS
Mass spectrometric fragmentation
Oxidation
Reduction

ABSTRACT

Lytic polysaccharide monooxygenases (LPMOs) are powerful enzymes that degrade recalcitrant polysaccharides, such as cellulose. However, the identification of LPMO-generated C1- and/or C4-oxidised oligosaccharides is far from straightforward. In particular, their fragmentation patterns have not been well established when using mass spectrometry. Hence, we studied the fragmentation behaviours of non-, C1- and C4-oxidised cello-oligosaccharides, including their sodium borodeuteride-reduced forms, by using hydrophilic interaction chromatography and negative ion mode collision induced dissociation - mass spectrometry. Non-oxidised cello-oligosaccharides showed predominantly C- and A-type cleavages. In comparison, C4-oxidised ones underwent B-/Y- and X-cleavage close to the oxidised non-reducing end, while closer to the reducing end C-/Z- and A-fragmentation predominated. C1-oxidised cello-oligosaccharides showed extensively A-cleavage. Reduced oligosaccharides showed predominant glycosidic bond cleavage, both B-/Y- and C-/Z-, close to the non-reducing end. Our findings provide signature mass spectrometric fragmentation patterns to unambiguously elucidate the catalytic behaviour and classification of LPMOs.

1. Introduction

An important step in the valorisation of lignocellulose is the enzymatic degradation of the (hemi-)cellulosic fraction into fermentable monosaccharides (Ragauskas et al., 2006). Hereto, hydrolytic polysaccharide degrading enzymes were considered unique for a long time. Therefore, they are abundantly present in commercial enzyme cocktails. Nevertheless, lytic polysaccharide monooxygenases (LPMOs) have been shown to boost hydrolases via oxidative cleavage of β -(1→4)-linkages in recalcitrant polysaccharides, such as cellulose, in the last decade (Forsberg et al., 2011; Hemsworth et al., 2015; Horn et al., 2012; Vaaje-Kolstad et al., 2010). This boosting effect has been explained by the fact that LPMOs generate new chain ends for hydrolases to act on and it has been suggested that LPMOs improve the substrate's accessibility for hydrolases as well (Harris et al., 2010; Horn et al.,

2012; Martinez, 2016; Villares et al., 2017).

LPMOs have been shown to vary in their regioselectivity, which means that they are either specifically oxidising the C1- or the C4-carbon position in polysaccharides. In addition, less regioselective LPMOs have been described able to oxidise both C1- and C4-carbon positions (Frommhagen et al., 2018). Due to the oxidation of either the C1- or the C4-position, the corresponding glycosidic linkage becomes unstable leading to its cleavage, and, thus, eventually LPMO catalysis leads to formation of both oxidised and non-oxidised oligosaccharides (Beeson et al., 2012; Beeson et al., 2015; Kim et al., 2014). The action of C1-directed LPMOs results in release of unstable 8-lactones, which further undergo a ring cleavage in aqueous solution leading to the formation of aldonic acids. The action of C4-directed LPMOs generate 4-ketoaldoses, which might hydrate to their corresponding geminal diols in the presence of water (Isaksen et al., 2014; Westereng et al.,

Abbreviation: ESI-CID-MS/MS, electrospray ionisation - collision induced dissociation - mass spectrometry; Mt, *Myceliophthora thermophila* C1; LPMO, lytic polysaccharide monooxygenase; PGC, porous graphitic carbon chromatography; RP-UHPLC, reversed phase - ultra high performance liquid chromatography; HILIC, hydrophilic interaction chromatography; HPAEC-PAD, high performance anion exchange chromatography with pulsed amperometric detection; NaBH₄, sodium borohydride; NaBD₄, sodium borodeuteride; RAC, regenerated amorphous cellulose; Asc, ascorbic acid; SPE, solid phase extraction; FA, formic acid; TFA, trifluoroacetic acid; DP, degree of polymerisation; Glc_n, non-oxidised cello-oligosaccharides; Glc_n^{*}, C4-oxidised cello-oligosaccharides; Glc_n[#], C1-oxidised cello-oligosaccharides; RD-Glc_n, reduced (alditol forms of) non-oxidised cello-oligosaccharides; RD-Glc_n^{*}, reduced (alditol forms of) C4-oxidised cello-oligosaccharides

* Corresponding author.

E-mail addresses: peicheng.sun@wur.nl (P. Sun), matthias.frommhagen@wur.nl (M. Frommhagen), maloe.kleinehaar@wur.nl (M. Kleine Haar), gijs.vanerven@wur.nl (G. van Erven), edwin.bakx@wur.nl (E.J. Bakx), willem.vanberkel@wur.nl (W.J.H. van Berkel), mirjam.kabel@wur.nl (M.A. Kabel).

<https://doi.org/10.1016/j.carpol.2020.115917>

Received 1 November 2019; Received in revised form 13 January 2020; Accepted 24 January 2020

Available online 26 January 2020

0144-8617/© 2020 The Authors. Published by Elsevier Ltd. This is an open access article under the CC BY-NC-ND license (<http://creativecommons.org/licenses/by-nc-nd/4.0/>).

2016), but the latter is not always observed (Frommhagen et al., 2016).

The identification of these C1- and C4-oxidised carbohydrate structures is far from straightforward, albeit various analytical approaches have been developed as thoroughly reviewed previously (Eijsink et al., 2019; Monclaro & Filho, 2017). Among those analytical approaches, high performance anion exchange chromatography with pulsed amperometric detection (HPAEC-PAD) and matrix assisted laser desorption/ionisation - time of flight - mass spectrometry (MALDI-TOF-MS) are mostly used. Although HPAEC allows identification of LPMO-oxidised compounds based on their elution time, hereto, not commonly available standards of oxidised oligosaccharides products are required. The more complex the oxidised oligosaccharide are, which have been generated, for example LPMO-oxidised branched xyloglucano-oligosaccharides (Kojima et al., 2016; Ladeuze et al., 2017; Nekuinaite et al., 2016; Petrovic et al., 2018), the more challenging the identification of C1- or C4- (or both) oxidation is based on their elution time. MALDI-TOF-MS can be used to detect oxidised oligosaccharides based on *m/z* values, but the determination of C1- and C4-oxidised oligosaccharides is far from easy. MALDI-TOF-MS cannot distinguish isomers and specifically cannot distinguish i.e. the geminal diol form of C4-oxidised from the same oligosaccharide but C1-oxidised having the same *m/z* (Forsberg et al., 2011; Frommhagen et al., 2016; Frommhagen et al., 2015). Therefore, mixed C4-, C1- or both C1-/C4-oxidised oligosaccharides cannot be distinguished by this method. To overcome these challenges, other methods, which combine chromatography directly with mass spectrometry have been studied. Thus obtained mass spectrometric fragmentation patterns are seen as distinct signatures, and differ for each oligosaccharide structure (Chai et al., 2001; Kool et al., 2013; Pfenninger et al., 2002b; Westphal, Kuhnel et al., 2010; Westphal, Schols et al., 2010). Various attempts to separate and identify LPMO-generated oxidised products have been reported, for example by using reversed phase - ultra high performance liquid chromatography (RP-UHPLC), porous graphitic carbon chromatography (PGC) and hydrophilic interaction chromatography (HILIC) techniques connected to electrospray ionisation - collision induced dissociation - mass spectrometry (ESI-CID-MS/MS) (Bennati-Granier et al., 2015; Frommhagen, van Erven, et al., 2017; Isaksen et al., 2014; Westereng et al., 2016). However, most intriguingly, a systematic study to generate MS/MS fragmentation patterns of the different chromatographically separated C1- and C4-oxidised oligosaccharides has not been performed yet.

In a few studies, CID-MS/MS of oxidised cello-oligosaccharides has been performed, albeit mainly in the positive ion mode. The positive ion mode is known to provide multiple MS/MS fragments with high intensity, but the presence of multiple sodium (and ammonium) adducts complicates the spectra obtained (Deery et al., 2001; Harvey, 2000; Kailemia et al., 2014; Reis et al., 2003). Alternatively, CID-MS/MS of oligosaccharides can be performed in negative ion mode. This technique has been shown for non-oxidised oligosaccharides to give lower background noise, thus clearer spectra, and the fragmentation behaviours are suggested to be more specific and predictable (Chai et al., 1998; Chai et al., 2001; Gao et al., 2015; Harvey, 2005a, 2005b; Lawson et al., 1990).

Furthermore, reduction of oligosaccharides has been shown to assist in their unambiguous separation and identification. Well known is the sodium borohydride (NaBH₄) initiated reduction of oligosaccharides to avoid α / β -anomers in various chromatographic approaches and co-occurring loss of the signal (Abdel-Akher et al., 1951; Barr et al., 1996; Beeson et al., 2012; Hantus et al., 1997; Kawasaki et al., 2000; Mazumder & York, 2010; Vinogradov et al., 2002; York et al., 1996). At the same time, sodium borodeuteride (NaBD₄) has been shown to label the reducing end of carbohydrates, which is helpful for the structural determination of many different oligosaccharides (Ring & Selvendran, 1978; Selvendran & King, 1989; Xie et al., 2004).

In this study, we investigated the CID-MS/MS fragmentation patterns of non-oxidised, LPMO-generated C1- and C4-oxidised cel-

oligosaccharides in negative ion mode. Moreover, these cello-oligosaccharides were reduced by using NaBD₄ and fragmentation behaviours of the resulting oligosaccharides were studied. It is hypothesised that oxidised cello-oligosaccharides show distinct signature fragmentation patterns compared to their non-oxidised and reduced forms. Unambiguous signature fragmentation patterns of C1- and C4-oxidised cello-oligosaccharides will allow further understanding of LPMO mechanisms and their oxidised products.

2. Materials and methods

2.1. Carbohydrates, cellulose substrate and other chemicals

Galactose, NaBD₄ and ammonium acetate were purchased from Sigma-Aldrich (St. Louis, MO, USA). Cellobiose, cellotriose, cellotetraose, cellopentaose and cellohexaose were purchased from Megazyme (Bray, Ireland). Regenerated amorphous cellulose (RAC) was prepared from Avicel PH-101 (Sigma-Aldrich) as described previously (Frommhagen et al., 2015). Ascorbic acid (Asc) and sorbitol were purchased from VWR International (Radnor, PA, USA). All water used was produced by a Milli-Q system (Millipore, Molsheim, France), unless mentioned otherwise.

2.2. Generation of non-, C4- and C1-oxidised cello-oligosaccharides by *MtLPMO9E* and *MtLPMO9I* from RAC

RAC was suspended in 50 mM ammonium acetate buffer (pH 5.0) to a concentration of 2 mg/mL. Subsequently, each LPMO from *Myceliophthora thermophila* C1 (*MtLPMO9E* (MTCTH_79765, UniProt ID: G2Q7A5) and *MtLPMO9I* (MTCTH_2299721, UniProt ID: G2Q774)) was added to the corresponding RAC suspension (in the presence of 1 mM Asc (final concentration)) at a concentration of 2 μ M. The expression, production and purification of *MtLPMO9E* and *MtLPMO9I* together with determination of their protein content and purity are described in Supplementary information and Fig. S1. Control reactions were performed without the addition of Asc. *MtLPMO9E* incubations were carried out at 50 °C and those with *MtLPMO9I* at 30 °C by using an Eppendorf Thermomixer comfort, placed in a vertical direction, at 800 rpm (24 h reaction; 500 μ L total volume). All incubations were performed in duplicate. The reactions were stopped by immediately separating supernatants and pellets through centrifugation 22,000 \times g, 15 min, 4 °C in a table centrifuge. The resulting supernatants were collected and cleaned up directly or after reduction with solid phase extraction (SPE) as described in section 2.3 prior to analysis.

2.3. Reduction of non- and oxidised-cello-oligosaccharides with NaBD₄ and clean-up with SPE

Reduction was performed by adding 200 μ L freshly prepared 0.5 M NaBD₄ to 200 μ L of the standard mixture (containing cellobiose, cellotriose, cellotetraose, cellopentaose and cellohexaose, 50 μ g/mL each) and of supernatants obtained from the *MtLPMO9E*- and *MtLPMO9I*-RAC incubations at room temperature (20 °C) for 20 h. A clean-up procedure for reduced and non-reduced samples was carried out by using SPE with Supelclean™ ENVI-Carb™ columns (3 mL, Sigma-Aldrich). The SPE column was activated with 1.5 mL 80 % (v/v) acetonitrile in water with 0.1 % (v/v) trifluoroacetic acid (TFA), followed by adding three times 1.5 mL water. Samples were loaded on the column and washed four times with 1.5 mL water to remove unbound compounds. Bond oligosaccharides were eluted with two times 1.5 mL 60 % (v/v) acetonitrile in water with 0.05 % (v/v) TFA and the obtained samples were dried under a stream of nitrogen at room temperature (20 °C). The dried samples were dissolved in 50 μ L water prior to analysis.

2.4. Analytic methods

2.4.1. HPAEC-PAD analysis for profiling oligosaccharides

All samples, NaBD_4 -reduced and non-reduced forms of (SPE cleaned) cello-oligosaccharides having a degree of polymerisation (DP) of 2–6 and NaBD_4 reduced and non-reduced forms of (SPE cleaned) supernatants of RAC incubated with *MtLPMO9E* or *MtLPMO9I*, were analysed by using HPAEC with an ICS-5000 system (Dionex, Sunnyvale, CA, USA) equipped with a CarboPac PA-1 column (2 mm ID \times 250 mm; Dionex) in combination with a CarboPac PA guard column (2 mm ID \times 50 mm; Dionex). The system was further equipped with PAD. Two mobile phases were (A) 0.1 M NaOH and (B) 1 M NaOAc in 0.1 M NaOH were kept under helium flushing and the column temperature was 20 °C. The elution profile applied has previously been described (Frommhagen et al., 2016). Samples were diluted five times before analysis.

2.4.2. HILIC-ESI-CID-MS/MS for elucidating fragmentation patterns

Oligosaccharides in non-reduced and NaBD_4 -reduced forms of SPE-cleaned cello-oligosaccharides (DP 2–6) and NaBD_4 -reduced and non-reduced forms of SPE-cleaned supernatants of *MtLPMO9E*- or *MtLPMO9I*-incubated RAC samples were separated and analysed by using HILIC-ESI-CID-MS/MS. A Vanquish UHPLC system (Thermo Scientific, Waltham, MA, USA) equipped with an Acuity UPLC BEH Amide column (Waters, Millford, MA, USA; 1.7 μm , 2.1 mm ID \times 150 mm) and a VanGuard pre-column (Waters; 1.7 μm , 2.1 mm ID \times 150 mm) was used. The column temperature was set at 35 °C and the flow rate was 0.45 mL/min; injection volume was 2 μL . Water (A) and acetonitrile (B), both containing 0.1 % (v/v) formic acid (FA) (all were UHPLC-grade; Biosolve, Valkenswaard, The Netherlands) were used as mobile phases. The separation was performed by using the following elution profile: 0–2 min at 82 % B (isocratic), 2–42 min from 82 % to 60 % B (linear gradient), 42–42.5 min from 60 % to 42 % B (linear gradient), 42.5–49 min at 42 % B (isocratic), 49–50 min from 42 % to 82 % B (linear gradient) and 50–60 min at 82 % B (isocratic). The mass (m/z) of separated oligosaccharides was on-line detected by an LTQ Velos Pro mass spectrometer (Thermo Scientific) equipped with a heated ESI probe. MS data were obtained in negative ion mode with the following settings: source heater temperature 400 °C, capillary temperature 250 °C, sheath gas flow 50 units, source voltage 2.5 kV and m/z range 300–1500. As MS/MS settings, CID with a normalised collision energy was set at 35 %, with a minimum signal threshold of 5000 counts at an activation Q of 0.2 and activation time of 10 ms. Mass spectrometric data were processed by using Xcalibur 2.2 software (Thermo Scientific).

3. Results and discussion

3.1. Negative ion mode CID-MS/MS fragmentation of non-, C1- and C4-oxidised cello-oligosaccharides separated by HILIC

The aim of this research was to define specific signature fragmentation pathways for non-, C1- and C4-oxidised cello-oligosaccharides by using HILIC-ESI-CID-MS/MS in negative ion mode. The specific signature fragmentation patterns of the NaBD_4 -reduced forms of the non-, C1- and C4-oxidised oligosaccharides are discussed in section 3.2.

A mixture of commercially available non-oxidised cello-oligosaccharides with a DP of 2–6 (Glc_2–6) was used as the standard (Fig. S2 and S3). C4-oxidised cello-oligosaccharides (Glc_n*) were generated by incubating *MtLPMO9E* with RAC only when Asc was present (Fig. S2 and S3). We confirmed its C4-specific oxidative cleavage with previously reported data of other C4-specific LPMOs, in particular by comparison of HPAEC elution behaviours (Fig. S2) and MALDI-TOF mass spectra (Frommhagen et al., 2016; Frommhagen, van Erven, et al., 2017; Kadowaki et al., 2018). In addition to Glc_n* in the *MtLPMO9E*-RAC-digest, Glc_2–4 were also generated (Fig. S2, F and Fig. S3, B), which were confirmed by their elution time identical to the standards (Glc_2–4) by HPAEC (Fig. S2 and S3) and by their m/z -values in HILIC-ESI-MS (Fig. S4). C1-oxidised cello-oligosaccharides (Glc_n#) were generated by incubating RAC with *MtLPMO9I* in the presence of Asc. Notably, we discovered a new C1-specific LPMO (Fig. S2 and S3) and confirmed its regioselectivity based on the comparison with previously reported data of RAC incubated with C1-specific *MtLPMO9B* and *MtLPMO9D* (Frommhagen et al., 2016; Frommhagen, Westphal, et al., 2017). Apart from Glc_n#, Glc_2–6 were present in the *MtLPMO9I*-RAC-digest (Fig. S2, D and Fig. S3, C) and their identities were similarly defined as just described for the Glc_2–4 present in the *MtLPMO9E*-RAC-digest. It should be noted that minor peaks next to each DP of Glc_n were also observed of which the identities remain so far unknown. Although these minor peaks might be of utmost importance to understand LPMO's mode-of-action in more detail, their exact nature and significance are out of the scope of this research and not further studied here.

Mass spectra of Glc_n and Glc_n* analysed in full-scan mode with HILIC-ESI-MS indicated that these oligosaccharides were present mainly as their single charged deprotonated ($[\text{M} - \text{H}]^-$) and formate adducted ($[\text{M} + \text{FA} - \text{H}]^-$) products, while Glc_n# were present only in their $[\text{M} - \text{H}]$ -form (Fig. S4). In addition, the analysed m/z of Glc_n* (m/z -2 compared to the m/z of Glc_n of the same DP) indicated that the C4-oxidised cello-oligosaccharides were in their 4-ketoaldose form. Previously reported geminal diol forms of Glc_n* (m/z +16 compared to the m/z of Glc_n of the same DP (Isaksen et al., 2014; Westereng et al., 2016)) were not observed under the analytical conditions used. The Glc_n# were observed as aldonic acids based on their m/z -values (m/z +16 compared to the m/z of Glc_n of the same DP; Fig. S4). The

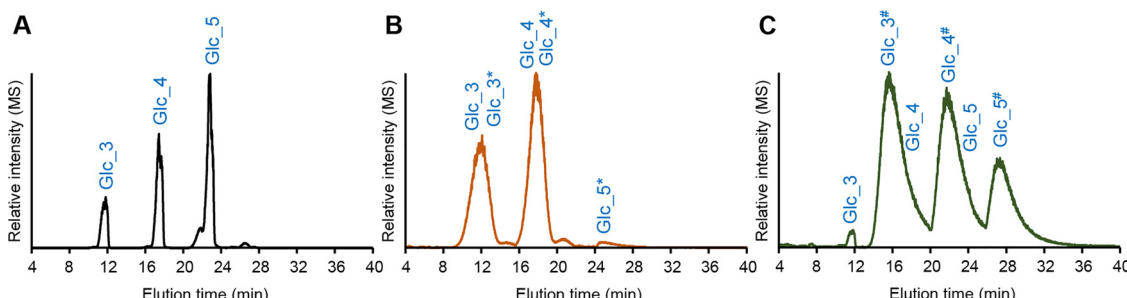


Fig. 1. HILIC extracted ion chromatograms of non-, C4- and C1-oxidised cello-oligosaccharides. (A) Non-oxidised cello-oligosaccharides: Glc_3, m/z 503.2; Glc_4, m/z 665.3; Glc_5, m/z 827.3; (B) Both non- and C4-oxidised cello-oligosaccharides: Glc_3–5 m/z see explanation panel A; Glc_3*, m/z 501.2; Glc_4*, m/z 663.3; Glc_5*, m/z 825.3; (C) Both non- and C1-oxidised cello-oligosaccharides: Glc_3–5, m/z see explanation panel A; Glc_3#, m/z 519.2; Glc_4#, m/z 681.3; Glc_5#, m/z 843.3. C4- and C1-oxidised cello-oligosaccharides were obtained from the incubation of RAC with either *MtLPMO9E* or *MtLPMO9I* in the presence of Asc (Fig. S2).

separation of DP3, 4 and 5 within Glc_n , Glc_n^* and $\text{Glc}_n^\#$ (Fig. 1), with well distinguishable m/z -values, allowed generation of their MS/MS fragmentation patterns. Hereto, the $[\text{M} - \text{H}]^-$ products were preferred, because fragmentation of $[\text{M} + \text{FA} - \text{H}]^-$ products was either not obtained or resulted in complex spectra with various formate adducted fragments.

The MS/MS spectra of DP3, 4 and 5 of non-oxidised cello-oligosaccharides (Glc_3 –5) are shown in Fig. S5 and annotated according to the nomenclature developed by Domon and Costello (1988). The MS/MS spectrum of Glc_3 (Fig. S5) showed two most abundant fragments Z_1 (m/z 161) and C_2 (m/z 341). The C_1 fragment (m/z 179) was also found but in lower abundance. Cross-ring fragments were seen from the ions $^{0,2}\text{A}_2$ (m/z 281) and $^{0,2}\text{A}_3$ (m/z 443), and with consecutive water loss from the ions $^{0,2}\text{A}_2$ ($^{0,2}\text{A}_2 - \text{H}_2\text{O}$, m/z 263) and $^{0,2}\text{A}_3$ ($^{0,2}\text{A}_3 - \text{H}_2\text{O}$, m/z 425). This further loss of a water molecule of $^{0,2}\text{A}_n$ fragments into $^{0,2}\text{A}_n - \text{H}_2\text{O}$ ions (or annotated as $^{2,5}\text{A}_n$ ions in some studies) has previously been shown to occur (Boulos & Nystrom, 2016; Mulroney et al., 1999; Quéméner et al., 2015). With increasing DP of non-oxidised cello-oligosaccharides (Glc_4 and Glc_5), C-type fragmentation was still predominant as shown by the pronounced relative intensity of C_2 (m/z 341), C_3 (m/z 503) and C_4 (m/z 665). In addition, the most abundant cross-ring fragments $^{0,2}\text{A}_n$ and $^{0,2}\text{A}_n - \text{H}_2\text{O}$ resulted from cleavages of the B ring (reducing end) and the B-neighbouring ring. Similar CID-MS/MS results of neutral $\beta(1 \rightarrow 4)$ linked gluco-oligosaccharides ($[\text{M} - \text{H}]^-$) with predominant C-type glycosidic cleavage and $^{0,2}\text{A}_n$ cross-ring fragmentation have been described (Chai et al., 1998; Palma et al., 2015; Pfenninger et al., 2002a; Quéméner et al., 2003). Although the MS/MS fragmentation patterns of Glc_n in negative ion mode can be found in literature, we still provided our MS/MS spectra of Glc_n here as the reference to better compare to the spectra of other types of cello-oligosaccharides.

The MS/MS fragmentation spectra of DP3 and DP4 of C4-oxidised cello-oligosaccharides (Glc_3^* and Glc_4^*) are shown in Fig. 2. The MS intensity of Glc_5^* was too weak to obtain decent MS/MS spectra, mainly due to the very low amount of Glc_5^* present in the *MtLPMO9E*-RAC-digest. Various attempts, for example increasing the dose of *MtLPMO9E*, were performed to increase the yield of Glc_5^* . However, the yield of Glc_5^* was not significantly improved (data not shown). It is thought that *MtLPMO9E* is able to cleave soluble cel-

oligosaccharides having DP larger than 5, which has been reported previously (Kadowaki et al., 2018; our *MtLPMO9E* is *MtLPMO9J* in this study). Nevertheless, to our opinion, the clear signature fragmentation behaviours and diagnostic fragments of DP3 and DP4 are representative for C4-oxidised cello-oligosaccharides in general. The MS/MS spectrum of Glc_3^* indicated B_1 (m/z 159) and C_1 (m/z 177) ions, which were m/z -2 compared to Z_1 (m/z 161) and Y_1 (m/z 179), indicating, as expected, that an oxidised glucosyl unit was present at the non-reducing end (A ring). MS/MS ring-fragments of Glc_3^* , $^{0,2}\text{A}_2$ (m/z 279) and $^{0,2}\text{A}_3$ (m/z 441; $^{0,2}\text{A}_3 - \text{H}_2\text{O}$, m/z 423) were also found, in decreasing abundance towards the A ring. Surprisingly, the fragment $^{2,4}\text{X}_2$ (m/z 281) was detected, which has barely been shown to occur in negative ion mode CID-MS/MS of oligosaccharides so far. Fragmentation of the C4-oxidised cellotriose apparently resulted in loss of the oxidised end via ring cleavage leading to a $^{2,4}\text{X}_2$ (m/z 281) fragment. In the MS/MS spectrum of Glc_4^* , the three most abundant fragments were B_1 (m/z 159), Y_2 (m/z 341) and Y_3 (m/z 503). Hence, B- and Y-type fragmentation preferably took place at the glycosidic linkage at the right side of the A and A neighbouring ring, most likely influenced by the C4-oxidised group. In contrast, pronounced ions of Z_1 (m/z 161), C_3 (m/z 501) and C_2 (m/z 339) suggested C- and Z-type fragmentation at the glycosidic linkage at the left side of the B ring, similar to the fragmentation of non-oxidised cello-oligosaccharides. This preference was further apparent from the very low intensity of C_1 (m/z 177), Y_1 (m/z 179), B_3 (m/z 483) and Z_3 (m/z 485) fragments. Likewise, for Glc_3^* , A- and X-type of cross-ring fragmentation of Glc_4^* was observed as $^{2,4}\text{X}_3$ (m/z 443) and $^{2,4}\text{X}_3 - \text{H}_2\text{O}$ (m/z 425). Hence, these $^{2,4}\text{X}_n$ fragments can be seen as diagnostic ions specifically for C4-oxidised cello-oligosaccharides. The intensity of the $^{2,4}\text{X}_n$ fragments decreased closer to the B ring, observed from the much lower relative intensity of $^{2,4}\text{X}_2$ (m/z 281) and $^{2,4}\text{X}_2 - \text{H}_2\text{O}$ (m/z 263). For the B ring and B neighbouring rings $^{0,2}\text{A}_n$ ($-\text{H}_2\text{O}$) fragments were predominant and decreased in intensity when situated closer to the A ring.

A summary of the MS/MS fragmentation patterns of the (C4-oxidised) cello-oligosaccharides, including signature fragments, is given in Table 1.

The MS/MS fragmentation of C1-oxidised cello-oligosaccharides (aldonic acids, $\text{Glc}_n^\#$, Fig. 3 and Fig. S6) was very distinct from the fragmentation obtained for Glc_n and Glc_n^* . In the $\text{Glc}_3^\#$ MS/MS

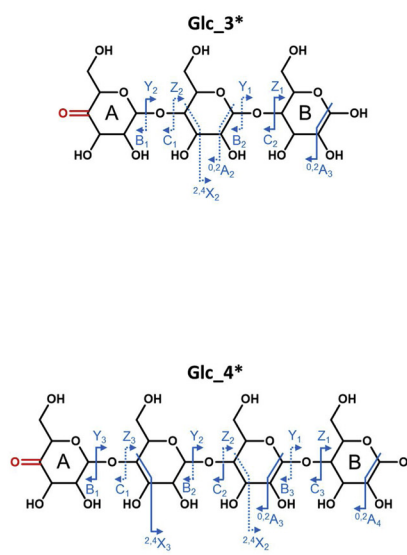
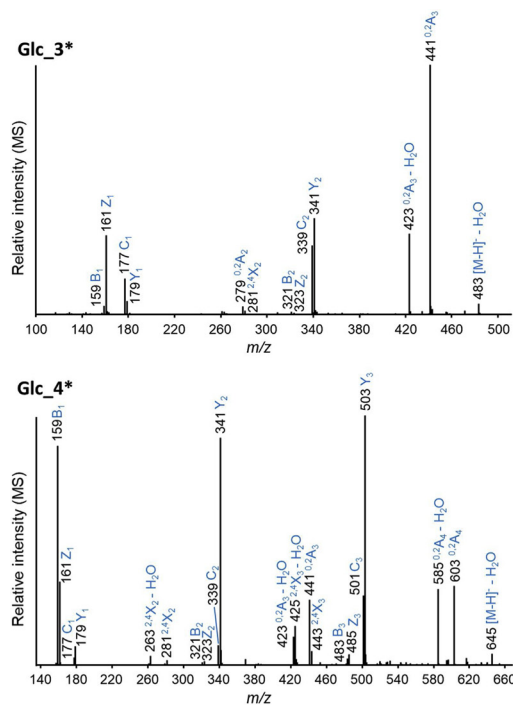


Fig. 2. Negative ion mode CID-MS/MS spectra of C4-oxidised cello-oligosaccharides DP3 and DP4 (Glc_3^* , m/z 501.2 and Glc_4^* , m/z 663.3); average spectra across chromatographic peaks. The fragments are annotated according to Domon and Costello (1988). Blue solid arrows indicate abundant fragments, while dashed arrows indicate fragments with a lower relative intensity. 4-keto groups are indicated in red. A and B ring represent the non-reducing and reducing end, respectively. C4-oxidised cello-oligosaccharides were generated by RAC incubated with *MtLPMO9E* in the presence of Asc (Fig. S2) (For interpretation of the references to colour in this figure legend, the reader is referred to the web version of this article).

Table 1

Summary of fragmentation patterns of five types of cello-oligosaccharides observed in HILIC-ESI-CID-MS/MS.

Sugar type	Structure (β -(1 \rightarrow 4)-glucosyl backbone)	Fragmentation patterns	
		Glycosidic bond cleavage	Cross-ring cleavage
Non-oxidised (Glc_n)		C-ions are predominant	$^{0,2}A_n$ - and $^{2,4}A_n$ -fragments; $^{0,2}A_n$ -fragments are predominant on B ring, but decreases closer to A ring; $^{2,4}A_n$ -fragments on B ring and B neighbouring ring
C4-oxidised (Glc_n*)		Both B-Y- and C-Z-fragments; B/Y-cleavage is predominant directly next to A ring, but decreases closer to B ring; C-Z-cleavage is predominant directly next to B ring but decreases closer to A ring	$^{2,4}X_n$ - and $^{0,2}A_n$ -fragments; $^{2,4}X_n$ -fragments are predominant on A ring, but decreases closer to B ring; $^{0,2}A_n$ -fragments are predominant on B ring, but decreases closer to A ring
C1-oxidised (Glc_n#)		Both B-Y- and C-Z-fragments; glycosidic bond cleavage is less pronounced compared to ring cleavage	$^{0,2}A_n$ -, $^{2,4}A_n$ - and little $^{(0,1)}A_n$ -fragments; $^{2,4}A_n$ -fragments are predominant (even over glycosidic bond cleavage) on the ring closed to B ring, but decreases closer to A ring
Reduced-non- oxidised (RD-Glc_n)		Both B-Y- and C-Z-fragments; glycosidic bond cleavage is predominant closer to A ring, but decreases closer to B ring	$^{0,2}A_n$ - and $^{2,4}A_n$ -fragments; not on A and B rings, but on the neighbouring rings of A and B
Reduced-C4- oxidised (RD-Glc_n*)		Both B-Y- and C-Z-fragments; glycosidic bond cleavage is predominant closer to A ring, but decreases closer to B ring	$^{0,2}A_n$ - and $^{2,4}A_n$ -fragments; not on A and B rings, but on the neighbouring rings of A and B

spectrum (Fig. 3), abundant B₁ (*m/z* 161) and C₁ (*m/z* 179) ions were observed, which represented the cleavage of the non-reducing end glucosyl unit (A ring). Apparently, glycosidic linkage cleavage next to, or in the neighbourhood of the aldonic acid residue was less favoured. In addition, A-type cross-ring fragments were detected, especially from cross-ring cleavage of the carboxyl end (B ring; $^{2,4}A_3$ (*m/z* 383)). Likewise for Glc₃[#], MS/MS of Glc₄[#] (Fig. 3) showed predominant cross-ring cleavage on the oxidised B ring and B neighbouring ring ($^{2,4}A_4$ (*m/z* 545) and $^{2,4}A_3$ (*m/z* 383), respectively; Table 1). Again $^{0,2}A_n$ (-H₂O) fragments were formed. Similarly, the MS/MS pattern of Glc₅[#] (Fig. S6) showed a series of $^{2,4}A_n$ and $^{0,2}A_n$ (-H₂O) fragments, which were predominant for the B ring and the B neighbouring ring (e.g. $^{2,4}A_4$, *m/z* 545 and $^{2,4}A_5$, *m/z* 707). Glycosidic bond cleavage still occurred but was relatively less abundant (Table 1). Although similar data for the MS/MS spectrum of Glc₃[#] has been reported previously by Boulos and

Nystrom (2016), the systematic fragmentation behaviours of a series of C1-oxidised cello-oligosaccharides is here presented for the first time.

3.2. Negative ion mode CID-MS/MS fragmentation of reduced non- and C4-oxidised cello-oligosaccharides separated by HILIC

Non- and C4-oxidised cello-oligosaccharides were successfully reduced by NaBD₄ to their alditol forms (RD-Glc_n and RD-Glc_n^{*}) and analysed by HPAEC (Fig. S7), while the obtained gluconic acid forms of the C1-oxidised cello-oligosaccharides cannot be reduced and remained in their aldonic acid form (Fig. S7). Through NaBD₄ reduction, the B ring of Glc_n was converted to the alditol form with one deuterium ion inserted, which led to *m/z* of 3 higher compared to the non-reduced Glc_n with the same DP (Fig. S8). Similarly to Glc_n, Glc_n^{*} were reduced at their reducing end, however, the C4-oxidised A ring was also

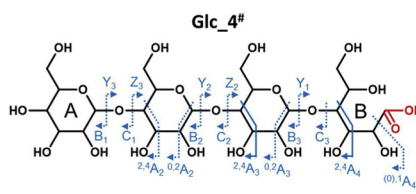
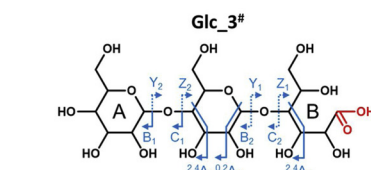
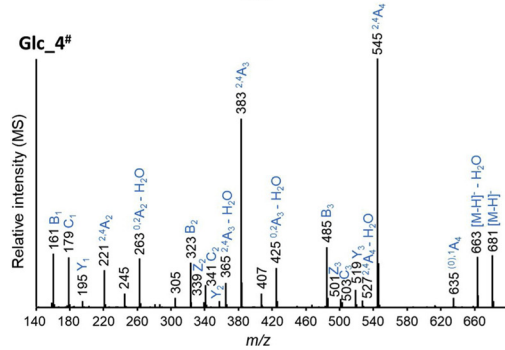
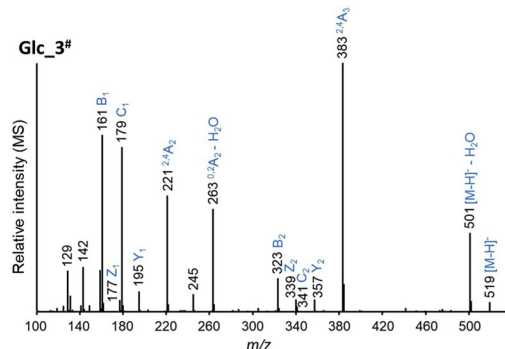


Fig. 3. Negative ion mode CID-MS/MS spectra of C1-oxidised cello-oligosaccharides DP3 (Glc₃[#], *m/z* 519.2) and DP4 (Glc₄[#], *m/z* 681.3). See Fig. S6 for DP5 (Glc₅[#], *m/z* 843.3); average spectra across chromatographic peaks. The fragments are annotated according to Domon and Costello (1988). Blue solid arrows indicate most abundant fragments, while dashed arrows indicate fragments with relatively lower intensity. Carboxyl groups are indicated in red. A and B ring represent the non-reducing and gluconic acid end, respectively. C1-oxidised cello-oligosaccharides were generated by RAC incubated with MtLPMO9I in the presence of Asc (Fig. S2) (For interpretation of the references to colour in this figure legend, the reader is referred to the web version of this article).

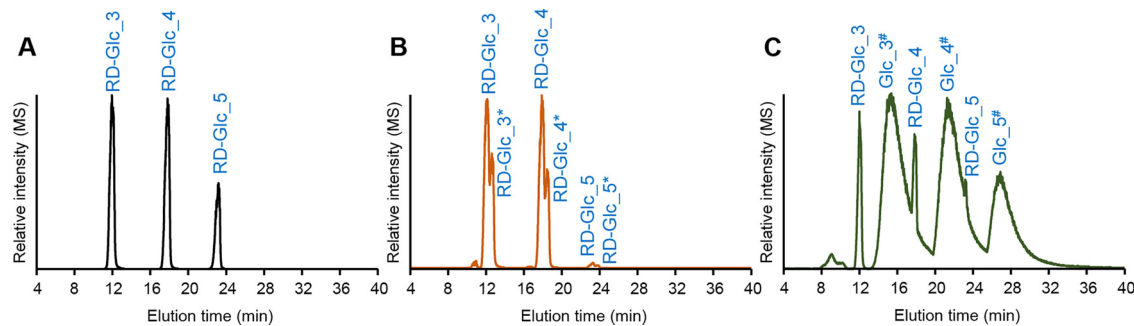


Fig. 4. HILIC extracted ion chromatograms of NaBD₄-reduced non-, C4- and C1-oxidised cello-oligosaccharides. (A) Reduced non-oxidised cello-oligosaccharides: RD-Glc₃, *m/z* 506.3; RD-Glc₄, *m/z* 668.3; RD-Glc₅, *m/z* 830.3; (B) Both reduced non- and C4-oxidised cello-oligosaccharides: RD-Glc₃₋₅, *m/z* see explanation panel A; RD-Glc_{3*}, *m/z* 507.2; RD-Glc_{4*}, *m/z* 669.3; RD-Glc_{5*}, *m/z* 831.3; (C) Reduced non- and C1-oxidised cello-oligosaccharides: RD-Glc₃₋₅, *m/z* see explanation panel A; Glc_{3#}, *m/z* 519.2; Glc_{4#}, *m/z* 681.3; Glc_{5#}, *m/z* 843.3.

reduced with addition of one deuterium ion, which was evident from the *m/z* observed. RD-Glc_{n*} resulted in a *m/z* of 4 higher compared to the non-reduced Glc_n with the same DP (Fig. S8). Constituent monosaccharide analysis after TFA hydrolysis showed that reduction of the A ring led the formation of glucosyl as well as galactosyl units (Fig. S9). HPAEC monosaccharide chromatograms clearly showed that galactose was generated in RD-Glc_{n*}, but not in RD-Glc_n after TFA hydrolysis. The generation of galactose after reduction of C4-oxidised cello-oligosaccharides and TFA hydrolysis was also described by Beeson et al. (2012). It can be hypothesised that the reduction of the C4-oxidised glucosyl residue leads to the formation of a hydroxyl group at the C4-carbon atom, whose conformational orientation is in equilibrium between the equatorial or axial position. The formation of the two types of RD-Glc_{n*} was also seen from the HPAEC chromatogram (Fig. S7). As RD-Glc_{n*} with glucosyl or galactosyl units have the same *m/z* values in HILIC-ESI-MS, we used RD-Glc_{n*} to indicate both (Fig. S8). RD-Glc₃₋₅ and RD-Glc_{3-5*} ([M - H]⁻) were well separated by HILIC (Fig. 4), allowing accurate characterisation of their MS/MS fragmentation behaviours. An overview of fragmentation behaviours of the reduced cello-oligosaccharides is shown in Table 1.

The MS/MS fragments of RD-Glc_n (Fig. 5 and Fig. S10) showed again distinct cleavage patterns. In the MS/MS spectrum of RD-Glc₃

(Fig. 5), B₁ (*m/z* 161) and C₁ (*m/z* 179) were abundant ions and mainly generated from the A ring. Closer to the B ring, glycosidic bond fragmentation was less pronounced indicated by the low relative intensity of B₂ (*m/z* 323) and C₂ (*m/z* 341). The same fragmentation was observed from the high relative intensity of Y₂ (*m/z* 344) and Z₂ (*m/z* 326) and low abundance of Y₁ (*m/z* 182). Cross-ring fragmentation occurred, mainly seen from ^{2,4}A₂ (*m/z* 221) and more abundant ^{0,2}A₂ - H₂O (*m/z* 263). RD-Glc₄ exhibited a similar trend of fragmentation as determined for RD-Glc₃ (Fig. 5). Again, glycosidic bond cleavage preferably occurred at the right side of the A ring and decreased closer to the B ring: Z₃ (*m/z* 488) and Y₃ (*m/z* 506) were the most abundant ions followed by Y₂ (*m/z* 344), B₁ (*m/z* 161) and C₁ (*m/z* 179). Cross-ring fragmentation (^{0,2}A_n and ^{2,4}A_n) was indicated, like for RD-Glc₃, but to a lesser extent. The MS/MS fragmentation patterns as described above were also obtained for RD-Glc₅ (Fig. S10), demonstrated by the abundant ions of Y₄ (*m/z* 668), Z₄ (*m/z* 650) and Y₃ (*m/z* 506) and relative low intensities of B₄ (*m/z* 647), B₃ (*m/z* 485), C₃ (*m/z* 503), B₂ (*m/z* 323) and Z₂ (*m/z* 326).

The MS/MS spectra of RD-Glc_{n*} (Fig. 6 and Fig. S11) displayed overall the same patterns and fragmentation behaviour as obtained for RD-Glc_n, which can be expected given their almost identical structures after reduction. The only difference is the deuterium ion at the C4-

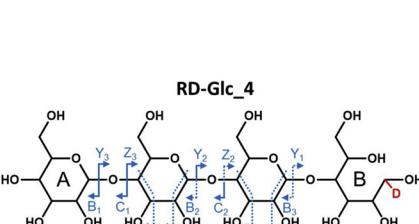
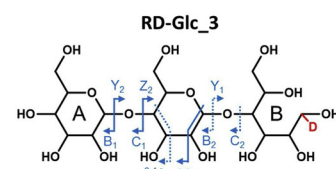
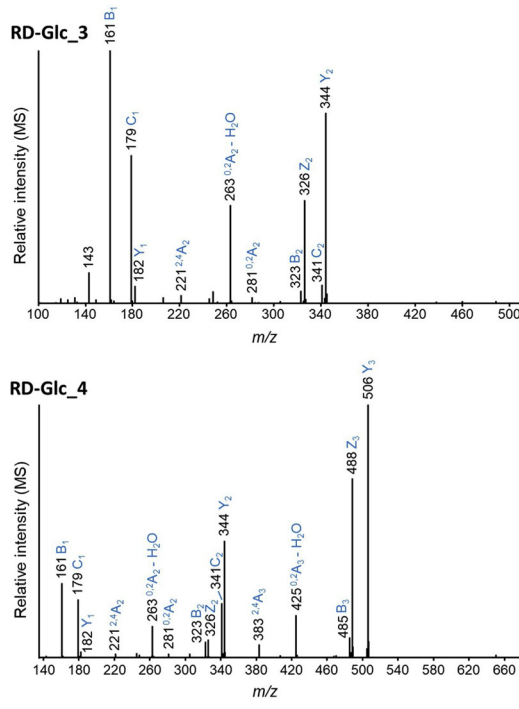
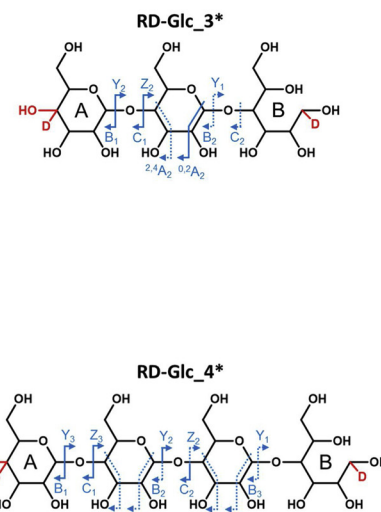
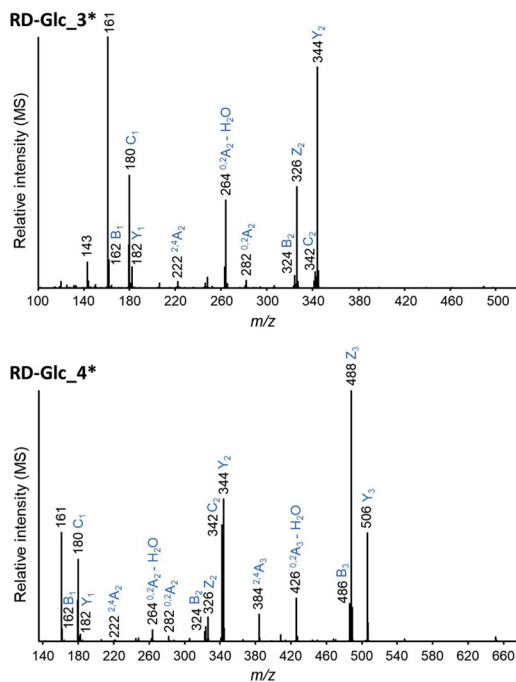


Fig. 5. Negative ion mode CID-MS/MS spectra of reduced non-oxidised cello-oligosaccharides DP3 (RD-Glc₃, *m/z* 506.3) and DP4 (RD-Glc₄, *m/z* 668.3). See Fig. S10 for DP5 (RD-Glc₅, *m/z* 830.3); average spectra across chromatographic peaks. The fragments are annotated according to Domon and Costello (1988). Blue solid arrows indicate the most abundant fragments, while dashed arrows indicate fragments with relatively lower intensity. The deuterium ion is indicated in red. A and B ring represent the non-reducing and deuterated alditol end, respectively (For interpretation of the references to colour in this figure legend, the reader is referred to the web version of this article).



position of the glucosyl A ring of RD-Glc_n* compared to the hydrogen ion for the RD-Glc_n oligosaccharides, resulting in A ring fragments of $m/z + 1$. This mass difference in the ions containing the A ring still allowed to distinguish RD-Glc_n from RD-Glc_n*. As indicated above, reduction also formed A ring galactosyl units, which could have potentially influenced the MS/MS fragmentation patterns of RD-Glc_n*. Yet, due to co-elution these effects cannot be further specified and the absence of cross-A-ring fragments furthermore does not allow to distinguish both structures.

Ions of m/z 162, 180, 324 and 342 in RD-Glc₃* (Fig. 6) were annotated as B₁, C₁, B₂ and C₂, respectively, as they obtained $m/z + 1$ compared to the ions generated from RD-Glc₃. Similarly, fragments of m/z 222, 264 and 282 were determined to be 2,4A₂, 0,2A₂ - H₂O and 0,2A₂, respectively. The similar MS/MS fragments having $m/z + 1$ were also found in RD-Glc₄* (Fig. 6) and RD-Glc₅* (Fig. S11) compared to the corresponding annotated ions in RD-Glc₄ and RD-Glc₅, respectively. In the MS/MS spectra of RD-Glc₃* and RD-Glc₄*, m/z 161 was unexpectedly more abundant than the B₁ ions (m/z 162). It is hypothesised that m/z 161 came from the internal glucosyl ions resulting from a double cleavage on RD-Glc_n*. Such double cleavage generating internal glucosyl ions (m/z 161) can also occur for RD-Glc_n, but cannot be distinguished from its B₁ ion (m/z 161). This double cleavage has been previously shown on other types of gluco-oligosaccharides in negative ion mode, such as carbohydrate chains of glycoproteins having 3-linked N-acetylglucosamine units and endoglucanase-digested xyloglucan-oligosaccharides (Chai et al., 2001; Quéméner et al., 2015).

In summary, the five types of cello-oligosaccharides analysed showed distinct fragmentation patterns in HILIC-separated negative ion mode CID-MS/MS (Table 1). In general, both glycosidic bond cleavage and cross-ring fragmentation occurred, though they were found to be rather different for each type of cello-oligosaccharide. Predominant C- and 0,2A_n (- H₂O)-fragments were found for non-oxidised cello-oligosaccharides, as also widely described in literature. C4-oxidised cello-oligosaccharides obtained predominant B-/Y-type fragmentation on the oxidised A ring while C-/Z-fragments were pronounced on the reducing end B ring. Notably, diagnostic 2,4X_n (- H₂O)-ions were annotated for the first time, which distinguish C4-oxidised cello-oligosaccharides from other ones. Extensive A-type cross-ring fragmentation over glycosidic bond cleavage was found in C1-oxidised cello-oligosaccharides, which is a unique feature of these particular cello-oligosaccharides.

Fig. 6. Negative ion mode CID-MS/MS spectra of reduced C4-oxidised cello-oligosaccharides DP3 (RD-Glc₃*, m/z 507.2) and DP4 (RD-Glc₄*, m/z 669.3). See Fig. S11 for DP5 (RD-Glc₅*, m/z 831.3); average spectra across chromatographic peaks. The fragments are annotated according to Domon and Costello (1988). Blue solid arrows indicate the most abundant fragments, while dashed arrows indicate fragments with relatively lower intensity. The formation of hydroxyl groups from the 4-keto groups and deuterium ions are indicated in red. A and B ring represent the non-reducing and deuterated alditol end, respectively. Note that the A-ring can represent a glucosyl and galactosyl unit (For interpretation of the references to colour in this figure legend, the reader is referred to the web version of this article.).

Though reduced non- and C4-oxidised cello-oligosaccharides showed identical fragmentation patterns, their structures can be distinguished by the different masses of ions containing the A ring. Compared to their non-reduced forms, reduced non- and C4-oxidised cello-oligosaccharides showed preferred glycosidic bond cleavage closer to the A ring.

4. Conclusions

In this study, fragmentation patterns of non-, C1- and C4-oxidised cello-oligosaccharides released by LPMOs and the reduced forms of non- and C4-oxidised cello-oligosaccharides were analysed by using HILIC-ESI-CID-MS/MS in negative ion mode. All type of cello-oligosaccharides showed both glycosidic bond and cross-ring cleavage fragments, but the fragmentation pattern of each type is distinct. Based on the outcomes of this research, also other structures of different oligosaccharides containing a β -(1 \rightarrow 4)-glucosyl (cellulose-like) backbone, for example branched oxidised xyloglucan-oligosaccharides, can be elucidated by their diagnostic ions and the specific fragmentation patterns. The structural elucidation of these complex (oxidised) oligosaccharides will further help understanding the mode-of-action of LPMOs regarding their ability to oxidatively degrade a range of plant cell wall polysaccharides, including cellulose and xyloglucan. Moreover, it can be envisaged that beyond the LPMO-field, our study contributes to the characterisation of (chemically) oxidised oligosaccharides in general.

Declaration of Competing Interest

The authors declare that they have no competing interest. All authors contributed to this study. Peicheng Sun, Matthias Frommhagen, Willem J.H. van Berkel and Mirjam A. Kabel contributed to the conception and design. Peicheng Sun, Matthias Frommhagen, Maloe Kleine Haar and Gijjs van Erven developed the methodology and carried out the experiments. Peicheng Sun and Edwin J. Bakx performed the data analysis. Peicheng Sun and Mirjam A. Kabel prepared the original draft. All authors were involved in critically reviewing all data and in writing the final manuscript. All authors read and approved the final manuscript.

Acknowledgements

The authors thank Sandra W. A. Hinz and Martijn J. Koetsier for their help in producing the LPMO enzymes (Genencor International B.V). Mark G. Sanders and Margaret Bosveld (Wageningen University & Research) are acknowledged for their help with HILIC-ESI-CID-MS/MS and HPAEC, respectively. We gratefully thank Madelon Logtenberg and Henk A. Schols (Wageningen University & Research) for the discussion on the reduction of cello-oligosaccharides.

Appendix A. Supplementary information

Supplementary material related to this article can be found, in the online version, at doi:<https://doi.org/10.1016/j.carbpol.2020.115917>.

References

Abdel-Akher, M., Hamilton, J. K., & Smith, F. (1951). The reduction of sugars with sodium borohydride. *Journal of the American Chemical Society*, *73*, 4691–4692.

Barr, B. K., Hsieh, Y. L., Ganem, B., & Wilson, D. B. (1996). Identification of two functionally different classes of exocellulases. *Biochemistry*, *35*, 586–592.

Beeson, W. T., Phillips, C. M., Cate, J. H., & Marletta, M. A. (2012). Oxidative cleavage of cellulose by fungal copper-dependent polysaccharide monooxygenases. *Journal of the American Chemical Society*, *134*, 890–892.

Beeson, W. T., Vu, V. V., Span, E. A., Phillips, C. M., & Marletta, M. A. (2015). Cellulose degradation by polysaccharide monooxygenases. *Annual Review of Biochemistry*, *84*, 923–946.

Bennati-Granier, C., Garajova, S., Champion, C., Grisel, S., Haon, M., Zhou, S., & Berrin, J. G. (2015). Substrate specificity and regioselectivity of fungal AA9 lytic polysaccharide monooxygenases secreted by *Podospora anserina*. *Biotechnology for Biofuels*, *8*, 90.

Boulos, S., & Nystrom, L. (2016). UPLC-MS/MS investigation of beta-glucan oligosaccharide oxidation. *Analyst*, *141*, 6533–6548.

Chai, W., Luo, J., Lim, C. K., & Lawson, A. M. (1998). Characterization of heparin oligosaccharide mixtures as ammonium salts using electrospray mass spectrometry. *Analytical Chemistry*, *70*, 2060–2066.

Chai, W., Piskarev, V., & Lawson, A. M. (2001). Negative-ion electrospray mass spectrometry of neutral underivatized oligosaccharides. *Analytical Chemistry*, *73*, 651–657.

Deery, M. J., Stimson, E., & Chappell, C. G. (2001). Size exclusion chromatography/mass spectrometry applied to the analysis of polysaccharides. *Rapid Communications in Mass Spectrometry*, *15*, 2273–2283.

Domon, B., & Costello, C. E. (1988). A systematic nomenclature for carbohydrate fragmentations in FAB-MS/MS spectra of glycoconjugates. *Glycoconjugate Journal*, *5*, 397–409.

Eijsink, V. G. H., Petrovic, D., Forsberg, Z., Mekasha, S., Rohr, A. K., Varnai, A., & Vaaje-Kolstad, G. (2019). On the functional characterization of lytic polysaccharide monooxygenases (LPMOs). *Biotechnology for Biofuels*, *12*, 58.

Forsberg, Z., Vaaje-Kolstad, G., Westereng, B., Bunaes, A. C., Stenstrom, Y., MacKenzie, A., & Eijsink, V. G. H. (2011). Cleavage of cellulose by a CBM33 protein. *Protein Science*, *20*, 1479–1483.

Frommhagen, M., Koetsier, M. J., Westphal, A. H., Visser, J., Hinz, S. W., Vincken, J.-P., & Gruppen, H. (2016). Lytic polysaccharide monooxygenases from *Myceliphthora thermophila* C1 differ in substrate preference and reducing agent specificity. *Biotechnology for Biofuels*, *9*, 186.

Frommhagen, M., Sforza, S., Westphal, A. H., Visser, J., Hinz, S. W., Koetsier, M. J., & Kabel, M. A. (2015). Discovery of the combined oxidative cleavage of plant xylan and cellulose by a new fungal polysaccharide monooxygenase. *Biotechnology for Biofuels*, *8*, 101.

Frommhagen, M., Westphal, A. H., Van Berkel, W. J., & Kabel, M. A. (2018). Distinct substrate specificities and electron-donating systems of fungal lytic polysaccharide monooxygenases. *Frontiers in Microbiology*, *9*, 1080.

Frommhagen, M., van Erven, G., Sanders, M., van Berkel, W. J. H., Kabel, M. A., & Gruppen, H. (2017). RP-UHPLC-UV-ESI-MS/MS analysis of LPMO generated C4-oxidized gluco-oligosaccharides after non-reductive labeling with 2-aminobenzamide. *Carbohydrate Research*, *448*, 191–199.

Frommhagen, M., Westphal, A. H., Hilgers, R., Koetsier, M. J., Hinz, S. W. A., Visser, J., & Kabel, M. A. (2017). Quantification of the catalytic performance of C1-cellulose-specific lytic polysaccharide monooxygenases. *Applied Microbiology and Biotechnology*, *102*, 1281–1295.

Gao, C., Zhang, Y., Liu, Y., Feizi, T., & Chai, W. (2015). Negative-ion electrospray tandem mass spectrometry and microarray analyses of developmentally regulated nitrins based on Type 1 and Type 2 backbone sequences. *Analytical Chemistry*, *87*, 11871–11878.

Hantus, S., Pauly, M., Darvill, A. G., Albersheim, P., & York, W. S. (1997). Structural characterization of novel 1-galactose-containing oligosaccharide subunits of jojoba seed xyloglucans. *Carbohydrate Research*, *304*, 11–20.

Harris, P. V., Welner, D., McFarland, K. C., Re, E., Navarro Poulsen, J. C., Brown, K., & Lo Leggio, L. (2010). Stimulation of lignocellulosic biomass hydrolysis by proteins of glycoside hydrolase family 61: Structure and function of a large, enigmatic family. *Biochemistry*, *49*, 3305–3316.

Harvey, D. J. (2000). N-(2-diethylamino)ethyl-4-aminobenzamide derivative for high sensitivity mass spectrometric detection and structure determination of N-linked carbohydrates. *Rapid Communications in Mass Spectrometry*, *14*, 862–871.

Harvey, D. J. (2005a). Fragmentation of negative ions from carbohydrates: Part 2. Fragmentation of high-mannose N-linked glycans. *Journal of the American Society for Mass Spectrometry*, *16*, 631–646.

Harvey, D. J. (2005b). Fragmentation of negative ions from carbohydrates: Part 3. Fragmentation of hybrid and complex N-linked glycans. *Journal of the American Society for Mass Spectrometry*, *16*, 647–659.

Hemsworth, G. R., Johnston, E. M., Davies, G. J., & Walton, P. H. (2015). Lytic polysaccharide monooxygenases in biomass conversion. *Trends in Biotechnology*, *33*, 747–761.

Horn, S. J., Vaaje-Kolstad, G., Westereng, B., & Eijsink, V. G. (2012). Novel enzymes for the degradation of cellulose. *Biotechnology for Biofuels*, *5*, 45.

Isaksen, T., Westereng, B., Aachmann, F. L., Agger, J. W., Kracher, D., Kittl, R., & Horn, S. J. (2014). A C4-oxidizing lytic polysaccharide monooxygenase cleaving both cellulose and cello-oligosaccharides. *Journal of Biological Chemistry*, *289*, 2632–2642.

Kadowaki, M. A., Várnai, A., Jameson, J.-K., Leite, A. E., Costa-Filho, A. J., Kumagai, P. S., & Eijsink, V. G. (2018). Functional characterization of a lytic polysaccharide monooxygenase from the thermophilic fungus *Myceliphthora thermophila*. *PLoS One*, *13*, e0202148.

Kailemia, M. J., Ruhaak, L. R., Lebrilla, C. B., & Amster, I. J. (2014). Oligosaccharide analysis by mass spectrometry: A review of recent developments. *Analytical Chemistry*, *86*, 196–212.

Kawasaki, N., Ohta, M., Hyuga, S., Hyuga, M., & Hayakawa, T. (2000). Application of liquid chromatography/mass spectrometry and liquid chromatography with tandem mass spectrometry to the analysis of the site-specific carbohydrate heterogeneity in erythropoietin. *Analytical Biochemistry*, *285*, 82–91.

Kim, S., Stahlberg, J., Sandgren, M., Paton, R. S., & Beckham, G. T. (2014). Quantum mechanical calculations suggest that lytic polysaccharide monooxygenases use a copper-oxyl, oxygen-rebound mechanism. *Proceedings of the National Academy of Sciences of the United States of America*, *111*, 149–154.

Kojima, Y., Várnai, A., Ishida, T., Sunagawa, N., Petrovic, D. M., Igarashi, K., & Yoshida, M. (2016). A lytic polysaccharide monooxygenase with broad xyloglucan specificity from the brown-rot fungus *Gloeophyllum trabeum* and its action on cellulose-xyloglucan complexes. *Applied and Environmental Microbiology*, *82*, 6557–6572.

Kool, M. M., Gruppen, H., Sworn, G., & Schols, H. A. (2013). Comparison of xanthans by the relative abundance of its six constituent repeating units. *Carbohydrate Polymers*, *98*, 914–921.

Ladeveze, S., Haon, M., Villares, A., Cathala, B., Grisel, S., Herpoel-Gimbert, I., & Berrin, J. G. (2017). The yeast *Geotrichum candidum* encodes functional lytic polysaccharide monooxygenases. *Biotechnology for Biofuels*, *10*, 215.

Lawson, A. M., Chai, W., Cashmore, G. C., Stoll, M. S., Hounsell, E. F., & Feizi, T. (1990). High-sensitivity structural analyses of oligosaccharide probes (neoglycolipids) by liquid-secondary-ion mass spectrometry. *Carbohydrate Research*, *200*, 47–57.

Martinez, A. T. (2016). How to break down crystalline cellulose. *Science*, *352*, 1050–1051.

Mazumder, K., & York, W. S. (2010). Structural analysis of arabinoxylans isolated from ball-milled switchgrass biomass. *Carbohydrate Research*, *345*, 2183–2193.

Monclaro, A. V., & Filho, E. X. F. (2017). Fungal lytic polysaccharide monooxygenases from family AA9: Recent developments and application in lignocellulose breakdown. *International Journal of Biological Macromolecules*, *102*, 771–778.

Mulrone, B., Barrie Peel, J., & Traeger, J. C. (1999). Theoretical study of deprotonated glucopyranosyl disaccharide fragmentation. *Journal of Mass Spectrometry*, *34*, 856–871.

Nekiunaita, L., Petrovic, D. M., Westereng, B., Vaaje-Kolstad, G., Hachem, M. A., Várnai, A., & Eijsink, V. G. (2016). FglLPMO9A from *Fusarium graminearum* cleaves xyloglucan independently of the backbone substitution pattern. *FEBS Letters*, *590*, 3346–3356.

Palma, A. S., Liu, Y., Zhang, H. T., Zhang, Y. B., McCleary, B. V., Yu, G. L., & Chai, W. G. (2015). Unravelling glucan recognition systems by glycome microarrays using the designer approach and mass spectrometry. *Molecular & Cellular Proteomics*, *14*, 974–988.

Petrovic, D. M., Bissaro, B., Chylenski, P., Skaugen, M., Sorlie, M., Jensen, M. S., & Eijsink, V. G. H. (2018). Methylation of the N-terminal histidine protects a lytic polysaccharide monooxygenase from auto-oxidative inactivation. *Protein Science*, *27*, 1636–1650.

Pfenninger, A., Karas, M., Finke, B., & Stahl, B. (2002a). Structural analysis of underivatized neutral human milk oligosaccharides in the negative ion mode by nano-electrospray MS⁽ⁿ⁾ (part 1: Methodology). *Journal of the American Society for Mass Spectrometry*, *13*, 1331–1340.

Pfenninger, A., Karas, M., Finke, B., & Stahl, B. (2002b). Structural analysis of underivatized neutral human milk oligosaccharides in the negative ion mode by nano-electrospray MS⁽ⁿ⁾ (part 2: Application to isomeric mixtures). *Journal of the American Society for Mass Spectrometry*, *13*, 1341–1348.

Quéméner, B., Désiré, C., Debrauwer, L., & Rathahao, E. (2003). Structural characterization by both positive and negative electrospray ion trap mass spectrometry of oligogalacturonans purified by high-performance anion-exchange chromatography. *Journal of Chromatography A*, *984*, 185–194.

Quéméner, B., Vigouroux, J., Rathahao, E., Tabet, J. C., Dimitrijevic, A., & Lahaye, M. (2015). Negative electrospray ionization mass spectrometry: A method for sequencing and determining linkage position in oligosaccharides from branched hemicelluloses. *Journal of Mass Spectrometry*, *50*, 247–264.

Ragauskas, A. J., Williams, C. K., Davison, B. H., Britovsek, G., Cairney, J., Eckert, C. A., & Tschaplinski, T. (2006). The path forward for biofuels and biomaterials. *Science*, *311*, 484–489.

Reis, A., Domingues, M. R. M., Domingues, P., Ferrer-Correia, A. J., & Coimbra, M. A.

(2003). Positive and negative electrospray ionisation tandem mass spectrometry as a tool for structural characterisation of acid released oligosaccharides from olive pulp glucuronoxylans. *Carbohydrate Research*, *338*, 1497–1505.

Ring, S. G., & Selvendran, R. R. (1978). Purification and methylation analysis of cell wall material from *Solanum tuberosum*. *Phytochemistry*, *17*, 745–752.

Selvendran, R. R., & King, S. E. (1989). Structural features of the cell-wall polysaccharides of the parchment layers of the pods of mature runner beans. *Carbohydrate Research*, *195*, 87–99.

Vaaje-Kolstad, G., Westereng, B., Horn, S. J., Liu, Z., Zhai, H., Sorlie, M., & Eijsink, V. G. (2010). An oxidative enzyme boosting the enzymatic conversion of recalcitrant polysaccharides. *Science*, *330*, 219–222.

Villares, A., Moreau, C., Bennati-Granier, C., Garajova, S., Foucat, L., Falourd, X., & Cathala, B. (2017). Lytic polysaccharide monooxygenases disrupt the cellulose fibers structure. *Scientific Reports*, *7*, 40262.

Vinogradov, E., Perry, M. B., & Conlan, J. W. (2002). Structural analysis of *Francisella tularensis* lipopolysaccharide. *European Journal of Biochemistry*, *269*, 6112–6118.

Westereng, B., Arntzen, M. O., Aachmann, F. L., Varnai, A., Eijsink, V. G., & Agger, J. W. (2016). Simultaneous analysis of C1 and C4 oxidized oligosaccharides, the products of lytic polysaccharide monooxygenases acting on cellulose. *Journal of Chromatography A*, *1445*, 46–54.

Westphal, Y., Kuhnel, S., Schols, H. A., Voragen, A. G., & Gruppen, H. (2010). LC/CE-MS tools for the analysis of complex arabino-oligosaccharides. *Carbohydrate Research*, *345*, 2239–2251.

Westphal, Y., Schols, H. A., Voragen, A. G., & Gruppen, H. (2010). Introducing porous graphitized carbon liquid chromatography with evaporative light scattering and mass spectrometry detection into cell wall oligosaccharide analysis. *Journal of Chromatography A*, *1217*, 689–695.

Xie, Y., Liu, J., Zhang, J., Hedrick, J. L., & Lebrilla, C. B. (2004). Method for the comparative glycomics analyses of O-linked, mucin-type oligosaccharides. *Analytical Chemistry*, *76*, 5186–5197.

York, W. S., Kolli, V. S. K., Orlando, R., Albersheim, P., & Darvill, A. G. (1996). The structures of arabinopyloglucans produced by solanaceous plants. *Carbohydrate Research*, *285*, 99–128.